

Digital holographic velocimetry with bacteriorhodopsin (BR) for real-time recording and numeric reconstruction

By D. H. Barnhart, N. Hampp*, N. A. Halliwell, and J. M. Coupland

Wolfson School of Mechanical and Manufacturing Engineering
Loughborough University, Loughborough, Leicestershire LE11 3TU, UK
e-mail correspondence: barnhart@wolfram.com

*Institute for Physical Chemistry, University of Marburg,
Hans-Meerwein-Strasse Geb. H, D-35032 Marburg, Germany

Abstract

Recent trends in other forms of optical metrology, such as particle image velocimetry (PIV), suggest that in order for holographic velocimetry (HV) to become a widespread tool, it must be based on digital recording without chemical development. While digital HV has been successfully demonstrated in recent years, unfortunately, the limited information capacity of present electronic sensors, such as CCD arrays, is still many orders of magnitude away from directly competing with high-resolution photographic film. As a result, present digital HV can not measure flows with volumetric dimensions larger than a few cubic millimeters. As a comparison, traditional photographic-based HV has an information capacity of more than a million cubic millimeters. In this paper, the authors report on the use of bacteriorhodopsin (BR) for digital HV that overcomes such limitations. In particular, BR is a real-time recording medium with an information capacity (5000 line-pairs/mm) that even exceeds high resolution photographic film. For digital HV, BR temporarily holds the hologram record so that its information content can be digitized for numeric reconstruction and displacement extraction. In many ways, BR appears ideally suited for digital HV. BR can deliver a reconstruction signal-to-noise ratio of 50 dB as well as an object-light recording sensitivity of 50 $\mu\text{J}/\text{cm}^2$ that corresponds with Agfa 8E56 holographic emulsions [Juchem and Hampp (2001)]. In contrast with photorefractive crystals, which have restricted apertures, BR holograms can be produced in large formats with large numeric apertures. Unlike thermoplastics, which can only support transmission holograms of restricted geometry, BR can be used in either reflection or transmission formats without restriction. Finally, unlike many real-time materials which have cycle-limited lifetimes, BR holograms can be recycled indefinitely without degradation.

Juchem T. and Hampp N. (2001) Optics Letters, vol 26, no 21, pp 1702-1704

1. Introduction

Recent trends in other forms of optical metrology, such as particle image velocimetry (PIV), suggest that in order for holographic velocimetry (HV) to become a widespread tool, it must be based on digital recording without chemical development. In recent years, digital holographic recording and reconstruction [Schnars *et al.* (1994)], digital holographic displacement measurement on micro-components [Seebacher *et al.* (1997)], and digital holographic velocity measurement in miniature-flows [Skarman *et al.* (1996), Skarman *et al.* (1999)] have all been successfully demonstrated. Unfortunately, the limited information capacity of present electronic sensors, such as CCD arrays, is still many orders of magnitude away from directly competing with high-resolution photographic film. As a result, present digital holography cannot take high-resolution measurements from objects with volumetric dimensions larger than a few cubic millimeters. Otherwise, the higher volumetric measurement size must be traded for diminished measurement accuracy. As a comparison, traditional photographic-based holography on a standard-sized plate of 100x100 square millimeters has an information capacity of more than a million cubic millimeters together with high numeric-aperture recording [Barnhart *et al.* (1994), Royer (1997)].

This paper introduces an approach that uses bacteriorhodopsin (BR) film as an intermediate information buffer to store the holographic information for further digital processing. In particular, BR is a real-time recording medium with an information capacity (5000 line-pairs/mm) that even exceeds high-resolution photographic film. For digital HV, BR temporarily holds the hologram record so that its information content can be digitized for numeric reconstruction and displacement extraction. In many ways, BR appears ideally suited for digital HV. BR can deliver a reconstruction signal-to-noise ratio of 50 dB as well as an object-light recording sensitivity of 50 uJ/cm² that corresponds with Agfa 8E56 holographic emulsion [Juchem and Hampp (2001)]. Although BR still has an overall light sensitivity requirement of ~1-5 mJ/cm², only 50 uJ/cm² needs to be present in the scattered object-light and the remainder of the energy can be placed in the reference beam. In contrast with photorefractive crystals, which have restricted apertures, BR holograms can be produced in large formats (100x100 mm²) with large numeric apertures. Unlike thermoplastics, which can only support transmission holograms of restricted geometry, BR can be used in either reflection or transmission formats without restriction. Finally, unlike many real-time materials which have cycle-limited lifetimes, BR holograms can be recycled indefinitely without degradation.

BR has a number of properties that are worth further consideration [Juchem and Hampp (2001)]. In general, BR holograms are usually recorded at a green (~532 nm) laser wavelength and erased with blue source of light that contains wavelengths between 400 and 450 nm. In general, it is not necessary for the erasing source to be coherent and, very often, a blue-filtered flash lamp is used. At room temperature, some BR forms will thermally decay with a half-life of about 100 seconds, although BR can be stable for hours at 0° C or even indefinitely for colder temperatures (<-20° C). When reconstructed at the 532 nm wavelength, BR works as an absorption hologram and has a diffraction efficiency of about one percent. While BR is not very sensitive to red wavelengths, such as 632 nm, it operates as a phase grating at these longer wavelengths and actually diffracts light much more strongly. Finally, BR has an interesting property in that it records and reconstructs the relative polarization of the object wavefront. This property can be exploited to increase the signal-to-noise ratio of the reconstruction or to record two independent, orthogonal-polarized holograms on the same BR plate.

There can be many different approaches for using BR to make digital recording and numeric reconstruction. The most general approach is to make a BR hologram recording and then take a digital scan of the recorded fringe information. This digitization process can be accomplished by either coherent or incoherent sampling of the hologram fringes. In either case, the BR hologram is digitized with a CCD camera by taking two-dimensional samples of the recorded wavefront at evenly spaced, overlapping intervals across the hologram aperture. Once digitized, these wavefront samples can then be converted into a complex-field and spliced together to recreate the recorded wavefront in the hologram. Once this has been accomplished, a digital Fresnel-transform can be applied to the numeric complex-field data in order to reconstruct the object information at a particular image plane and numerically investigate the image space within the computer's memory.

With incoherent sampling, the hologram is illuminated with an incoherent light source and very small patches of the recorded fringes on the hologram surface are incoherently imaged into a video

microscope at high magnification. This technique permits the BR hologram to be scanned at a wavelength that is different from the original recorded wavelength, which prevents the hologram from becoming erased during the digital scanning process. Unfortunately, such incoherent imaging procedures are resolution-limited by the point-spread function of the microscope imaging system. Another limitation is the short depth-of-focus tolerances of such high-magnification imaging systems. As a result, the scanning process must be tightly controlled to maintain a constant camera distance to the hologram surface throughout the scanning process. Finally, incoherent imaging can only be used with transmission holograms, but not reflection-hologram geometries, since reflection-hologram fringes cannot be incoherently imaged.

With coherent sampling, the hologram is reilluminated with a coherent light source and the hologram-diffracted wavefront at some known distance from the hologram is then magnified and digitized by mixing the diffracted wavefront with a known reference wavefront on the camera sensor-plane. In this case, the digitized wavefront need not coincide with the hologram surface and may be located at any chosen distance from the hologram. Unfortunately, however, the coherent light source generally needs to have the same wavelength as the recording laser to prevent unwanted distortion in the reconstructed wavefront. This has the unwanted consequence that the BR hologram is gradually erased by the reconstruction light source and added steps must be taken to minimize this effect. For example, a shuttered laser light source can be synchronized with the digitizing camera to avoid unnecessary light-exposure. In addition, an image-intensified camera may be also used to reduce the reconstruction energy requirements. Aside from these drawbacks, coherent-sampled holograms have the big advantage in that the fringe sampling procedures are not resolution-limited by aberrations in the digital imaging system. In particular, if the transfer-function of the imaging system can be accurately characterized, then the effects of aberrations present in the coherent imaging process can be later removed from the digitized wavefront data. In addition, both transmission and reflection hologram geometries may be used with coherent reconstruction methods.

While both of the coherent and incoherent-sampled methods previously mentioned are worthy of further consideration, the remainder of this paper will examine a recently-developed special form of coherent-sampled digitization that is known as object-conjugate reconstruction (OCR) [Barnhart (2001), Barnhart *et al.* (2002a)]. Object-conjugate reconstruction is distinctive from other coherent sampling methods in that the digitization camera optics can remain fixed, while an optical fiber probe is instead used to select the object-wavefront sample positions. This lightweight probe can be moved with speed across the sampled object-space. Furthermore, in its most basic form OCR does not rely on an external reference wavefront for the digitization process but instead measures the phase difference between two displaced object wavefronts rather than absolute phase information. With the basic OCR method, the each digitized sample contains an independent displacement measurement. In this case, the probe-sampled measurements do not cover the entire hologram aperture, but are instead taken at discrete, three-dimensional coordinates to directly correspond with displacement measurement locations. This results in a greatly reduced space-bandwidth requirement on the digitization process, by a factor as much as 1000, in comparison with the previously mentioned techniques that splice contiguous wavefront samples together.

2. Digital holographic displacement measurement in bacteriorhodopsin (BR) using object-conjugate reconstruction (OCR)

The basic OCR technique is shown schematically in Figure 1. First, a single plate, double-exposure reflection hologram is recorded by using two identical but laterally displaced converging reference beams at two different time instants, t_1 and t_2 . Then, the hologram is reconstructed using a diverging wave from a fiber-optic probe, which is placed in the original object space. This OCR configuration behaves as an imaging system such that a magnified image of the object space in the region of the probe is produced at two fixed points in space defined by the two previous points of focus of the recording reference beams [Barnhart *et al.* (2002a)]. Analogous to methods used in planar PIV [Adrian (1986)], the resulting reconstruction introduces a constant shift between exposures that provides a known bias displacement. This image shift not only resolves directional ambiguity of the object displacement, but also is essential if the object displacement is purely in the z (longitudinal) direction.

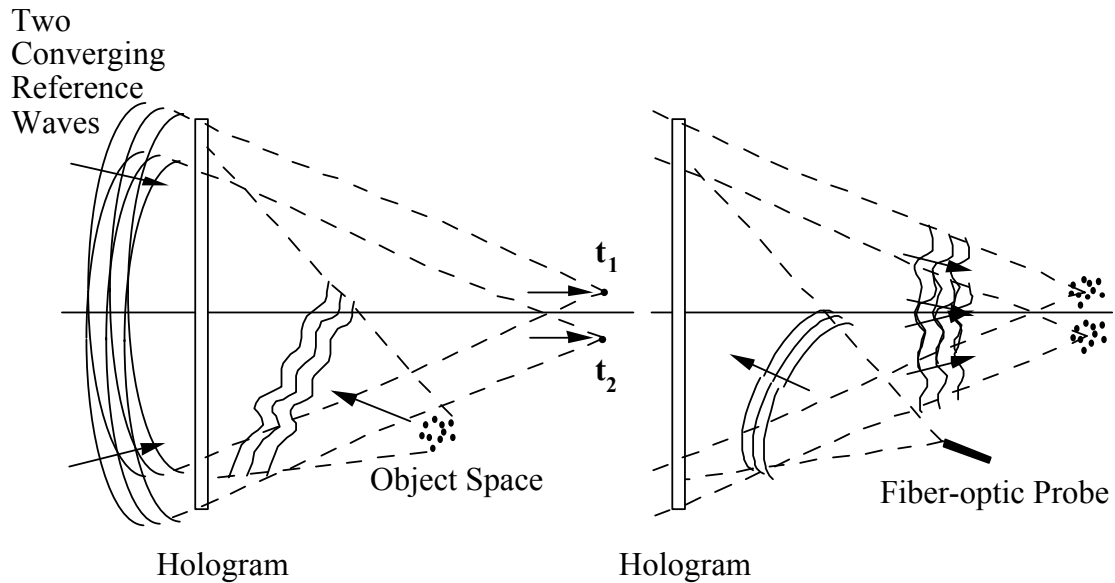


Figure 1. (a) Recording of hologram.

(b) Object-conjugate reconstruction of hologram.

For reconstruction, the double-exposed hologram is placed in a stand-alone displacement measurement assembly, depicted in Figure 2. Here, an optical fiber, which is mounted on a three-axis motorized translation stage and placed in the object volume, reilluminates the measurement hologram, which now diffracts the two displaced real images into the space surrounding the focal points of the original recording reference beams (located after the object space). A stationary pinhole aperture is located at the reference focus, followed with a Fourier transform lens and CCD camera. After each displacement measurement, the optical fiber is stepped through the larger object space (test volume) of interest, progressively sampling at selected points in space. A significant benefit of this arrangement is the fact that the pinhole-lens-camera remains stationary while the lightweight, movable optical fiber position determines the sample measurement coordinates. Moreover, complex-correlation analysis is inherently tolerant of image aberration effects since the complex correlation method directly processes the power spectrum of the object field, which is insensitive to phase aberrations [Coupland and Halliwell (1997)]. This means that simple reflection geometry holograms can be recorded ensuring high numeric-aperture recordings. The use of reflection geometries, until now, were precluded since they are the most prone to image aberration [Kocher (1988)].

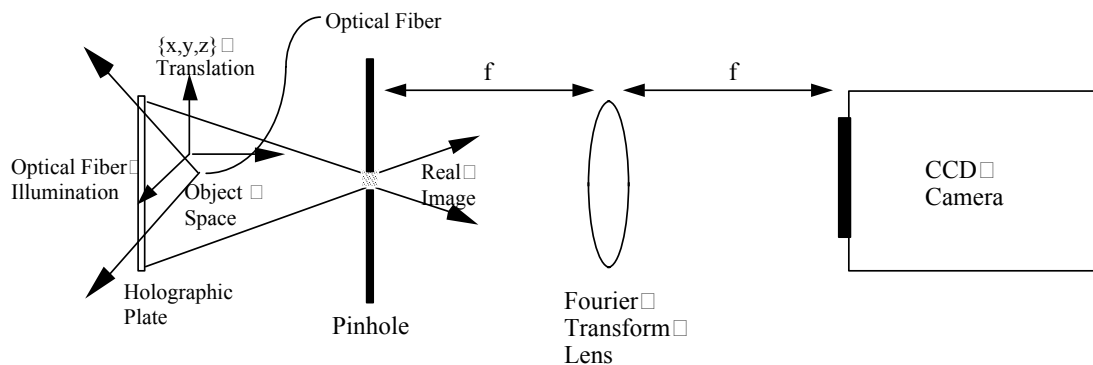


Figure 2. Reconstruction geometry with fiber optic illumination probe.

As illustrated in Figure 3, the real image formed within the pinhole opening determines the sample volume of a measurement point. After the optical Fourier transform, as shown in Figure 4, the CCD camera detects the two-dimensional power spectrum of the complex field emanating from the aperture [Goodman (1968)]. Ultimately, each sampled spatial power spectrum contains the necessary information to make a single three-dimensional vector displacement measurement [Coupland and Halliwell (1992)]. In practice, the digitized spatial power spectrum of each measurement sample is stored as an image file on a computer and its three-dimensional displacement is extracted by numeric processing methods to be discussed in the next section of this paper.

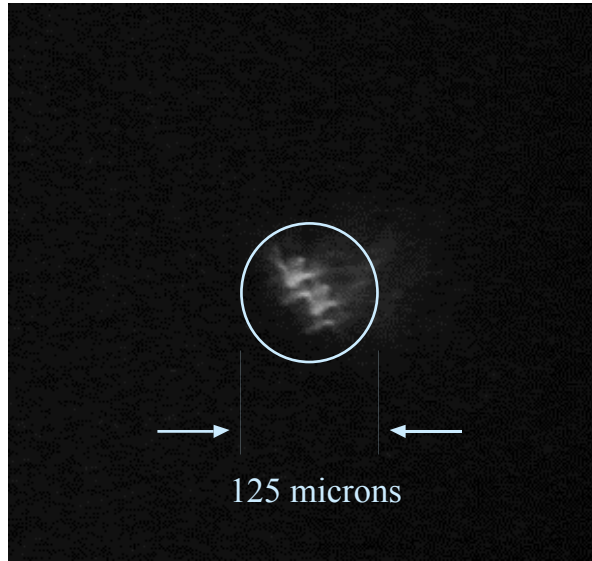


Figure 3. Holographic image formed at the pinhole.

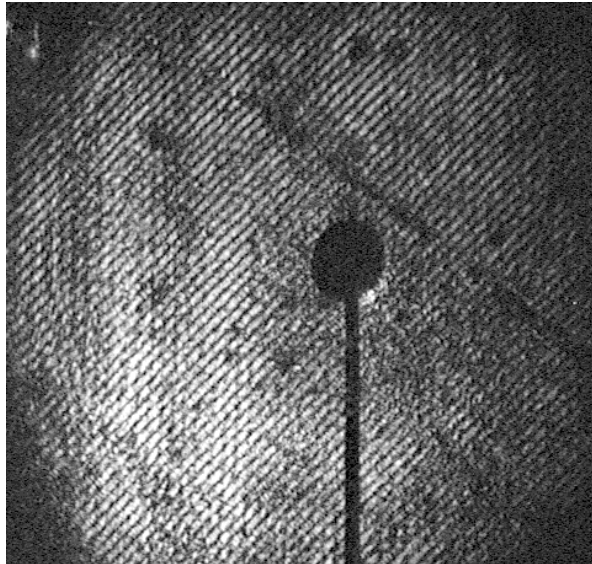


Figure 4. Resulting spatial power spectrum from Fourier-transform of reconstructed field at the pinhole. The spatial power spectrum consists of fringes generated by the interference between the displaced optical fields (analogous to Young's fringes in two-dimensional processing).

3. Numeric reduction of digital holographic data using OCR

Figure 5 illustrates the nine numeric steps used for displacement extraction. Of particular interest is the progressive reduction in the data-array size that occurs during the course of the displacement extraction process. At the start, in step one, the real-numbered spatial power spectrum is 288x352 pixels in size. Soon, however, in step three, the array size has diminished to 144x178 pixels after the complex-Fourier transform has been taken and a single quadrant of complex-numbered array extracted. Finally, in step seven, the array size is reduced once again to 72x88 pixels after the image shift information has been removed from the complex-field data. This progressive decrease in the array size occurs without any reduction of displacement accuracy since the encoded-displacement information has been conserved throughout the process. In essence, the first seven steps in the extraction process have resulted in a purified form of encoded-displacement information. Because of this progressive reduction in data size, the overall displacement extraction time is also significantly reduced by a factor of typically 16.

After the spatial power spectrum has been sampled for step one, shown previously in Figure 4, the Fourier transform is taken (step two) and a single quadrant is isolated (step three), shown in Figure 6(a). This produces a three-dimensional complex correlation of the displaced reconstructed wavefronts [Coupland and Halliwell (1992)]. In the magnitude plots shown in Figure 6, the lowest displacement is located at the lower right of the plot corners and the correlation peak are located in the middle of the plot. In general, the complex-correlation function is focused in three-dimensions such that its projection in the Fourier plane is slightly out of focus. The position of the correlation peak in the Fourier plane is proportional to the transverse (x-y) object displacement and its focus spot-size in the Fourier plane relates to the out-of-plane (z) displacement component. In previous reports on OCR, the three-dimensional position of an optical correlation was directly measured via an optical processor for displacement extraction [Barnhart (2001), Barnhart *et al.* (2002a,b)]. Presently, however, we only make use of the correlation structure to get an estimate of the displacement in step eight. (In order to achieve better measurement accuracy, we use this displacement estimate in step nine as a starting point of a minimization procedure that fits a simulated field to the experimental data.)

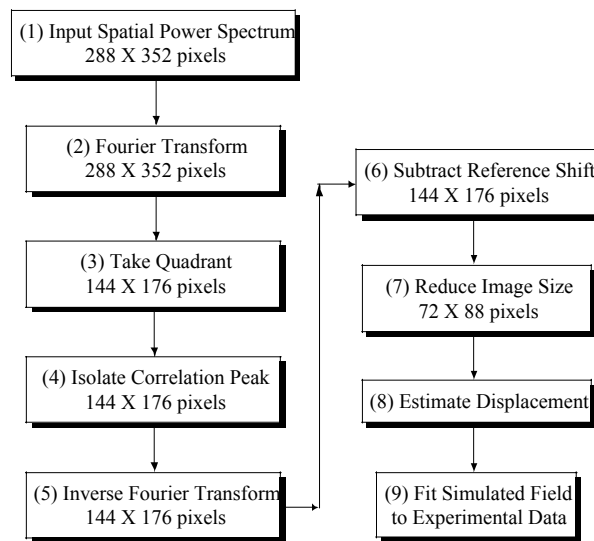


Figure 5. The nine steps of displacement extraction.

As discussed previously, OCR employs a form of image shifting to remove directional ambiguity from the displacement measurement. To accomplish this, as illustrated in Figure 1, two displaced reference beams were used during holographic recording whose displacement value was set to be greater than the maximum experimental displacement. As such, the two conjugate correlation peaks in the Fourier-transformed result of step two remain within their respective quadrant boundaries for all experimental displacement values and a single correlation peak can always be isolated for displacement extraction. This is achieved in the third step, shown in Figure 6(a), by retaining the fourth quadrant of the Fourier-transform plane such that a single correlation peak is present.

Following this step, the correlation centroid position is located and its spot size (second moment) is calculated in preparation for the fourth step. From this, shown in Figure 6(b), a Gaussian-window function, centered on the correlation and matched to its spot-size, is applied to the correlation space for step four in order to remove spurious peaks and noise in the correlation space.

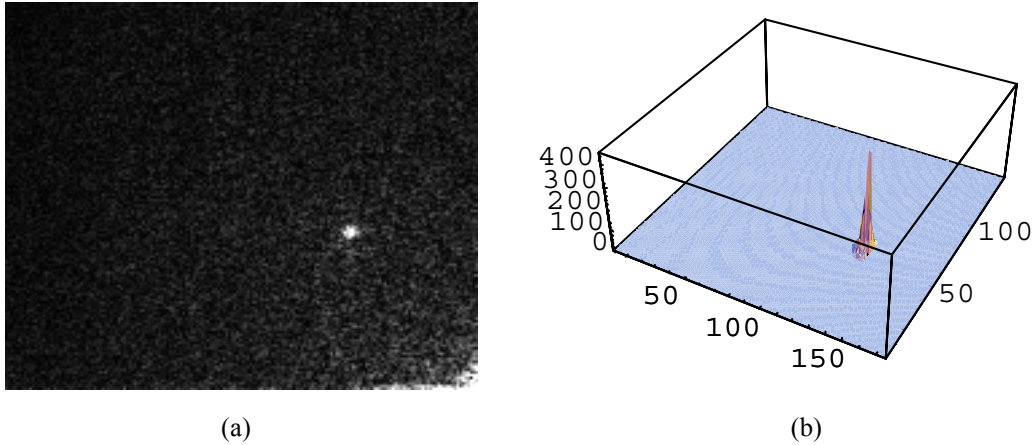


Figure 6. Isolation of complex correlation peak: (a) Isolated quadrant of Fourier transform magnitude, (b) Isolated correlation peak magnitude.

Following the application of steps one to four, Figure 7 depicts the next two steps of displacement extraction. As the fifth step, the inverse-Fourier transform, whose real values are plotted in Figure 7(a), is taken of the filtered correlation function, previously shown in Figure 6(b). At this stage, the complex-correlation result has been converted into a complex-field, $a(x, y)$, that contains the phase-difference between the two displaced object-wavefronts and can be represented by the following equation:

$$a(x, y) = \exp\left\{i\left[\frac{2\pi}{\lambda} \left(x_p x + y_p y + \frac{z_p^2}{2L} - \frac{x^2 + y^2}{2L} \right) + \phi \right]\right\}$$

where $\{x, y, z\}$ is the object displacement, $\{x_p, y_p, z_p\}$ denotes the fiber probe position, λ is the optical wavelength, $\{x, y\}$ are the hologram surface coordinates, and ϕ contains the phase contribution from the illumination beam (to be discussed later).

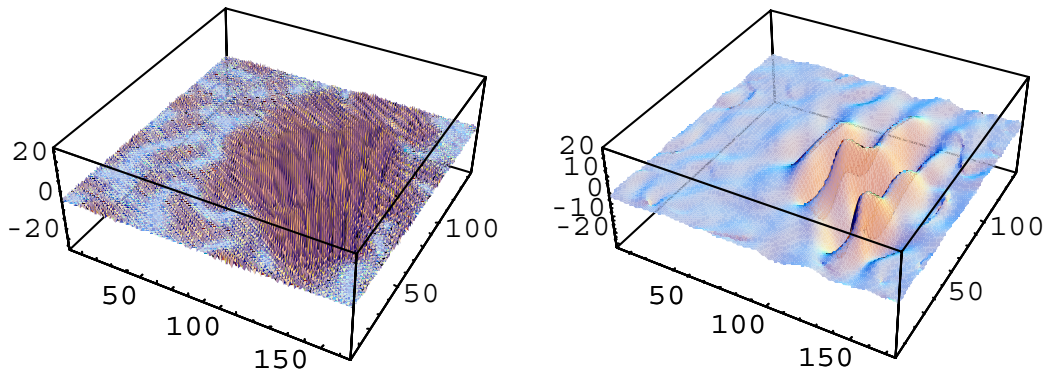


Figure 7. Manipulation of complex field: (a) Inverse-Fourier transform of isolated correlation, (real plot). (b) Complex-field result following phase reference removal, (real plot).

At first, the image-shift is still included in the object displacement. As revealed in Figure 7(a), this displacement magnitude is larger than the physical object displacement alone and gives rise to correspondingly higher spatial-frequencies. Therefore, as shown in Figure 7(b), the sixth step is to remove the image shift from the complex-field data. In practice, this is accomplished by use of a reference displacement measurement that was previously taken from either a stationary object point or a central-located point on the dynamically moving object in the hologram. First, the reference field, $r(x, y)$, is extracted from the reference measurement by repeating steps one through five with the reference measurement, analogous to $a(x, y)$. Finally, this reference field, $r(x, y)$, is used to remove the image shift from the displacement measurement by a multiplication between $a(x, y)$ and the complex conjugate of $r(x, y)$.

In general, it is only necessary to take a reference measurement from a single point in the object space. The resulting reference field, $r(x, y)$, can then be applied to all further displacement measurements in

the hologram. This is valid because the image shift remains constant for all points in the object space [Barnhart et al. (2002a)]. Also note that in addition to removing the image-shift, this reference measurement can remove any reference-beam phase distortion present in the holographic recording. In particular, the twin pulsed-YAG laser systems that are typically used in holographic velocimetry can have significantly different beam characteristics between their two channels and this imparts the two reference beams with different phase characteristics. However, by subtracting the reference data information from the displacement hologram data, such phase differences between the two reference beams are also removed. Finally, the use of such reference data eliminates the need for the user to have precise knowledge of the image-shift used in making the hologram, since the reference data inherently possesses this information.

Once the reference information has been subtracted from the complex-field data (Figure 7(a)) the remaining bandwidth is reduced and the resulting field information (Figure 7(b)) is now oversampled. Therefore, in step seven, the size of the dataset is further reduced from 144x176 pixels down to its final size of 72x88 pixels.

After the initial seven steps have been completed, the resulting complex-field data contains refined phase-difference information about the two displaced object wavefronts. The task now remains to use this phase information to extract the three components of object displacement. This is accomplished by first making an initial estimate of the object displacement, for step eight, using the Fourier-plane correlation result discussed previously, and then, in step nine, using this estimate as initial conditions in a numeric minimization to find the displacement parameters that best fit the phase-difference data. Once the object displacement has been estimated in step eight, the final step is to accurately determine the object displacement by fitting an analytic model of the complex amplitude, given by the previous equation for $a(x,y)$ (without image-shift), to the experimental data returned from step seven. In practice, this equation is built into a merit function that calculates the correlation between the extracted measurement field (depicted in Figure 7(b)) for any given displacement $\{?x, ?y, ?z\}$. This merit function is iteratively minimized, using the estimated displacement as the starting condition, to fit the best correlated displacement. Four examples of such fitted results are presented in Figure 8.

Here, the final object displacement parameters, $\{?x, ?y, ?z\}$, are iteratively changed until the best fit is found with the experimental data. The phase value, ϕ , in the equation for $a(x, y)$ contains the phase contribution of the illumination beam. When the illumination-beam phase characteristics are not accurately known, ϕ is simply fitted to the experimental data as an additional parameter. However, if the illumination phase contribution can be accurately characterized as a function of object position and object displacement, then ϕ can be defined as a function of object position and displacement. In such an event, the obtained measurement accuracy for $?z$ can actually be better than $?x$ and $?y$.

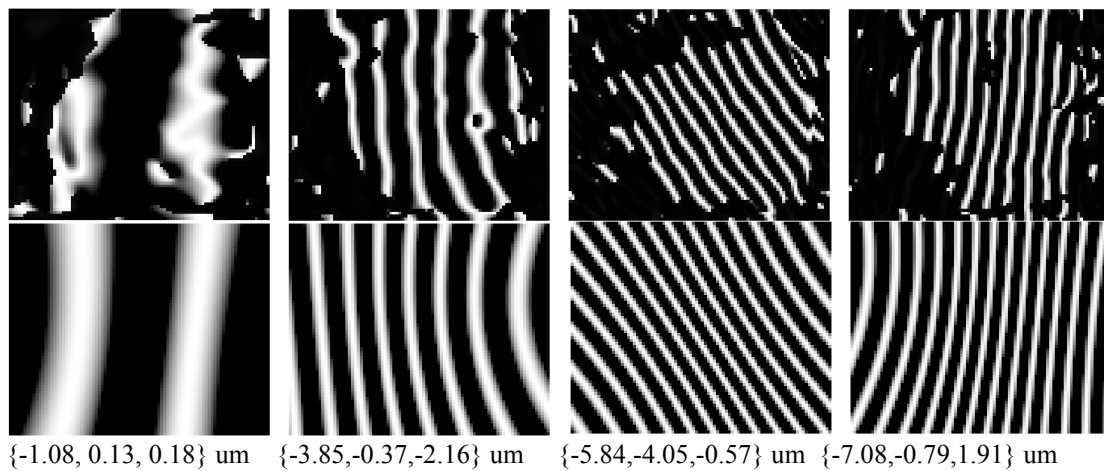


Figure 8. Some examples of sampled OCR measurements: The top images show the actual field measurements (real values shown). The middle images depict the corresponding fitted analytic models (real values shown). The bottom row of numbers report the fitted object displacements, given as $\{?x, ?y, ?z\}$.

4. Experiment

The same basic OCR technique can be used in either three-dimensional displacement measurement on surfaces [Barnhart *et al.* (2002a)] or three-dimensional velocity-field measurement in fluids [Barnhart *et al.* (2002b)]. For this paper, as a prelude to digital holographic velocimetry measurement in fluids and in order to characterize its displacement measurement accuracy, we have applied the OCR technique with BR recording to the surface displacement measurement on a stressed cantilever beam. A plan view of the holographic camera recording arrangement for cantilever surface measurement by OCR is illustrated below in Figure 9. Here the object space is located immediately in front of the hologram, H. In a typical experimental setting, the object measurement space occupies a volume with its center located 100 mm in front of the hologram. For the object illumination, shown in the three-dimensional view of Figure 4 (b), the current experiment employs 90 degree side scattering by an expanded cw laser beam (532 nm) that is reflected by M0.

In this OCR camera system, two identical, but laterally displaced, converging reference beams are generated by a custom-built holographic optical element (HOE) in combination with two large condenser lenses, L5 and L6 (150 mm diameter). The HOE is used to correct for optical aberrations in both the experiment as well as residual aberrations present in lenses L5 and L6. In addition, the HOE contains two separate holograms that are alternately illuminated at two distinct Bragg-angles, defined by M1 and M2, at the two different time instants, t_1 and t_2 . (More recently, however, we have stopped using a HOE in order to conserve more laser energy, choosing instead to use higher quality reference-focus optics.) As typical values, the two converging reference beam foci are diagonally displaced (in equal x-y directions) by 175 microns at a distance of 425 millimeters in front of the holographic plate, H. (For simplicity, only a single converging beams is drawn for clarity.) The resulting OCR image shift has a corresponding object displacement of 41 microns along the transverse diagonal that corresponds to 29 microns in each of the x - y directions. The entire hardware control, data acquisition, and data processing for the experiment was fully automated with purpose-built code written in *Mathematica*: a platform-independent, language environment by Wolfram Research.

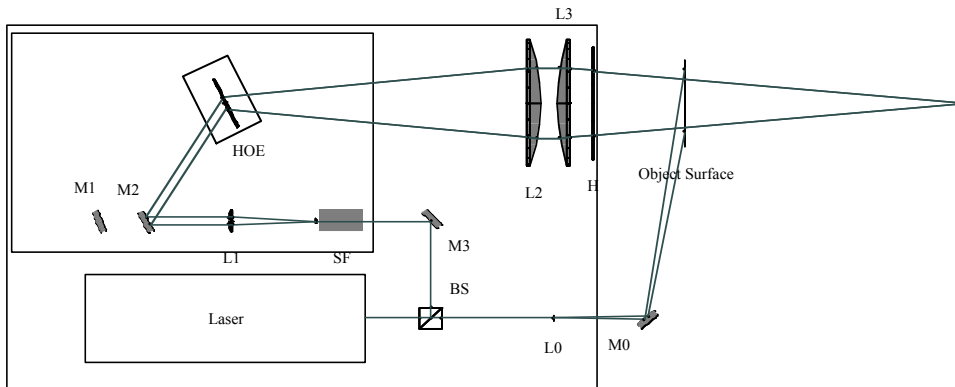


Figure 9. OCR camera for cantilever experiment.

5. Results

The resulting cantilever displacement measurement is shown in Figure 10. Here, the first four points were taken on the clamp that holds one side of the cantilever beam and the solid line shows the displacement predicted from cantilever theory [Benham and Warnock (1982)]. These results have a rms displacement resolution of 0.1 microns in the longitudinal directions (out-of-plane) and 0.05 microns in the transverse directions (in-plane) with a displacement range of ± 6 microns. This represents a dynamic range that is greater than 100:1 for the longitudinal component and greater than 200:1 for the transverse components of displacement. Because the principles of OCR can be applied to flow velocity measurement in same fashion as surface displacement measurement, the present reported results for surface displacement accuracy and dynamic range will also carry-through to future velocity-field measurements using OCR with BR recording.

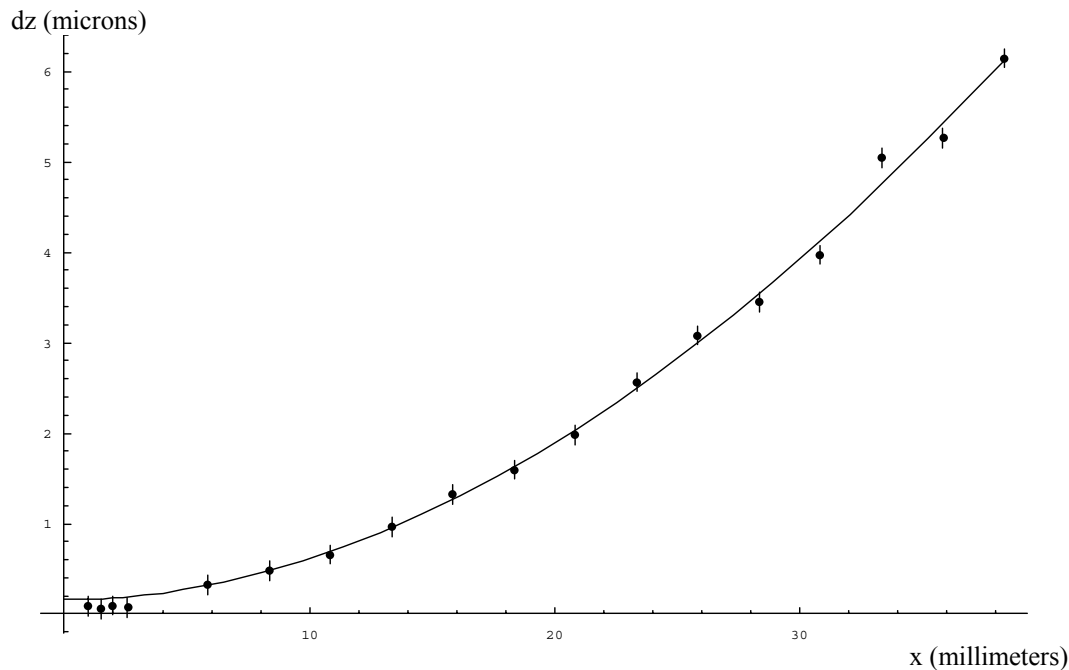


Figure 10. Digital holographic displacement measurement from cantilever beam by temporary storage in bacteriorhodopsin and numeric processing via OCR.

One of the greatest benefits of BR hologram recording is the fast turn-around time for an experimental measurement. Rather than requiring hours to conduct an experiment with wet-processed holography, the same experiment with BR holography can be accomplished in minutes. The cantilever result reported in Figure 10 was actually one of more than 50 distinct cantilever experiments conducted with our OCR system using BR holography over a period of a few days.

6. Conclusion

This paper has reported on the use of bacteriorhodopsin (BR) for digital holographic recording and numeric analysis. In particular, a cantilever experiment has been carried out in order to test the displacement measurement accuracy of BR. From this work, the rms accuracy of 0.1 microns and dynamic range of 100:1 for the longitudinal displacement component were obtained as well as the rms accuracy of 0.05 microns and dynamic range of 200:1 for the transverse components of displacement. In contrast with direct digital holography on CCD cameras, BR holograms are not restricted to microscopic object dimensions but, rather, can take volumetric measurements comparable with wet-processed holograms. Although not presented in this paper, we have recently successfully recorded BR holograms of 25-micron particles embedded in a block of plastic resin in order to confirm its ability for particle-field measurement. In the next experimental phase of this work, we shall be testing the use of BR recording with pulsed lasers and velocity-field measurement in fluids.

7. References

- Adrian R. J. (1986) "Image shifting technique to resolve directional ambiguity in double-pulsed velocimetry", *Applied Optics*, vol 25, pp 3855-3858.
- Barnhart D. H.; Adrian R. J.; Papen G. C. (1994) "Phase-conjugate holographic system for high-resolution particle-image velocimetry", *Applied Optics*, October 20, vol 33, no 30, pp 7159-7170.
- Barnhart D. H. (2001) *Whole-Field Holographic Measurements of Three-Dimensional Displacement in Solid and Fluid Mechanics*, PhD. thesis, Loughborough University, UK.
- Barnhart D. H.; Halliwell N. A.; Coupland J. M. (2002a) "Object Conjugate Reconstruction (OCR): A step forward in holographic metrology", *Proceedings of the Royal Society of London* (to appear).
- Barnhart D. H.; Chan V. S. S.; Halliwell N. A.; Coupland J. M. (2002b) "Holographic velocimetry using object-conjugate reconstruction (OCR): a new approach for simultaneous, 3-D displacement measurement in fluid and solid mechanics", *Experiments in Fluids* (to appear).
- Benham P. P. and Warnock F. V. (1982), *Mechanics of Solids and Structures*, Pitman International, Third Edition.

- Coupland J. M. and Halliwell N. A. (1992) "Particle image velocimetry: three-dimensional fluid velocity measurements using holographic recording and optical correlation", *Applied Optics*, March 10, vol 31, no 8, pp 1005-1007.
- Coupland J. M. and Halliwell N. A. (1997) "Holographic displacement measurements in fluid and solid mechanics: immunity to aberrations by optical correlation processing", *Proceedings of the Royal Society of London*, vol 453, pp 1053-1066.
- Goodman J. W. (1968) *Introduction to Fourier Optics*, McGraw Hill.
- Juchem T. and Hampp N. (2001), *Optics Letters*, vol 26, no 21, pp 1702-1704.
- Kocher C. (1988) *A Study of the Effects of Processing Chemistry of the Holographic Image Space*, PhD. thesis, Brighton Polytechnic, UK.
- Royer H. (1997) "Holographic and Particle Image Velocimetry", *Measurement Science Technology*, vol 8, pp 1562-1572.
- Schnars U. and Jüptner W. (1994), "Direct recording of holograms by a CCD target and numerical reconstruction", *Applied Optics*, January 10, vol 33, no 2, pp 179-181.
- Seebacher S.; Osten W.; Jüptner W. (1997), "3D-deformation analysis of micro-components using digital holography", *SPIE Proceedings Volume 3098*, pp 382-391.
- Skarman B.; Becker J.; Wozniak K. (1996), "Simultaneous 3D-PIV and temperature measurements using a new CCD-based holographic interferometer", *Flow Measurement and Instrumentation*, vol 7, no 1, pp 1-6.
- Skarman B.; Wozniak K.; Becker J. (1999), "Digital in-line holography for the analysis of Bénard-convection", *Flow Measurement and Instrumentation*, vol 10, pp 91-97.